



Kent Academic Repository

Wang, Yinan, Yao, Mingxi, Baker, Karen, Gough, Rosemarie E., Le, Shimin, Goult, Benjamin T and Yan, Jie (2021) *Force-dependent interactions between talin and full-length vinculin*. *Journal of the American Chemical Society*, 143 . pp. 14726-14737. ISSN 1520-5126.

Downloaded from

<https://kar.kent.ac.uk/89974/> The University of Kent's Academic Repository KAR

The version of record is available from

<https://doi.org/10.1021/jacs.1c06223>

This document version

Author's Accepted Manuscript

DOI for this version

Licence for this version

UNSPECIFIED

Additional information

Versions of research works

Versions of Record

If this version is the version of record, it is the same as the published version available on the publisher's web site. Cite as the published version.

Author Accepted Manuscripts

If this document is identified as the Author Accepted Manuscript it is the version after peer review but before type setting, copy editing or publisher branding. Cite as Surname, Initial. (Year) 'Title of article'. To be published in *Title of Journal*, Volume and issue numbers [peer-reviewed accepted version]. Available at: DOI or URL (Accessed: date).

Enquiries

If you have questions about this document contact ResearchSupport@kent.ac.uk. Please include the URL of the record in KAR. If you believe that your, or a third party's rights have been compromised through this document please see our [Take Down policy](https://www.kent.ac.uk/guides/kar-the-kent-academic-repository#policies) (available from <https://www.kent.ac.uk/guides/kar-the-kent-academic-repository#policies>).

Force-dependent interactions between talin and full-length vinculin

Yinan Wang¹, Mingxi Yao², Karen B. Baker³, Rosemarie E. Gough³, Shimin Le¹, Benjamin T. Goult^{3,*} and Jie Yan^{1,4,*}

¹Department of Physics, National University of Singapore, Singapore 117546.

²Department of Biomedical Engineering, Southern University of Science and Technology, P. R. China 518055

³School of Biosciences, University of Kent, Canterbury CT2 7NJ, UK

⁴Mechanobiology Institute, National University of Singapore, Singapore 117411.

* To whom the correspondence should be addressed: phyj@nus.edu.sg (YJ) or b.t.goult@kent.ac.uk (BTG).

KEYWORDS: *vinculin, talin, mechanical memory, autoinhibition, magnetic tweezers, mechanotransduction.*

ABSTRACT: Talin and vinculin are part of a multi-component system involved in mechanosensing in cell-matrix adhesions. Both exist in auto-inhibited forms, and activation of vinculin requires binding to mechanically activated talin, yet how forces affect talin's interaction with vinculin has not been investigated. Here by quantifying the force-dependent talin-vinculin interactions and kinetics using single-molecule analysis, we show that mechanical exposure of a single vinculin binding site (VBS) in talin is sufficient to relieve the autoinhibition of vinculin resulting in high-affinity binding. We provide evidence that the vinculin undergoes dynamic fluctuations between an auto-inhibited closed conformation and an open conformation that is stabilized upon binding to the VBS. Furthermore, we discover an additional level of regulation in which the mechanically exposed VBS binds vinculin significantly more tightly than the isolated VBS alone. Molecular dynamics simulations reveal the basis of this new regulatory mechanism, identifying a sensitive force-dependent change in the conformation of an exposed VBS that modulates binding. Together, these results provide a comprehensive understanding of how the interplay between force and autoinhibition provides exquisite complexity within this major mechanosensing axis.

Introduction

Integrin-mediated adhesions are multi-component molecular complexes that support the physical connection between cells and the extracellular matrix (ECM). At the core of these structures are the transmembrane integrins, α - β - heterodimers that bind ECM proteins through their large extracellular domains, and are connected to the intracellular actin cytoskeleton via adapter proteins such as

talin¹ and vinculin²⁻⁴. Integrin adhesions are required for cells to sense the rigidity of their microenvironment, which is important in a variety of processes including tissue formation, maintenance and repair^{5, 6}. Hence, understanding the fundamental mechanisms by which integrin adhesions sense and integrate mechanical signals is of crucial importance.

Talin plays a central role in integrin function and mechanosensing. By binding to β -

1
2
3 integrin tails through its N-terminal four-
4 point-one, ezrin, radixin, moesin (FERM)
5 domain, talin initiates inside-out integrin
6 activation^{7, 8}, while its large C-terminal rod
7 domain supports the connection between
8 integrins and F-actin⁹. When talin binds to
9 integrins at one end and to F-actin at the
10 other, it is mechanically stretched due to
11 actomyosin contraction¹⁰⁻¹³. Previous
12 studies have revealed that talin responds to
13 external forces by changing conformation
14 which in turn affects interactions with its
15 binding partners including vinculin¹⁴⁻²⁰.

21 Vinculin, a 116 kDa cytoplasmic protein,
22 has emerged as a key regulator of integrin
23 adhesions⁴. It acts in part by cross-linking
24 integrin-talin complexes to the actin
25 cytoskeleton⁴, and facilitates actin
26 polymerization and nucleation²¹. Hence,
27 vinculin plays a central role in cell adhesion
28 formation, maturation, and turnover²². Full-
29 length vinculin (FL-vinculin) is comprised of
30 five domains, D1, D2, D3, D4, which
31 together form the vinculin head that is
32 connected via a proline-rich linker to the
33 vinculin tail domain (Vt) (Fig. 1). Inter-
34 domain interactions within the vinculin
35 head organize the head into a pincer-like
36
37
38
39

structure^{23, 24} (Fig. 1). Vinculin binds to the
11 vinculin binding sites (VBSs) in the talin
rod via its D1 domain, and to F-actin
through Vt, and to numerous other
signaling proteins via interactions with
various domains^{2, 3, 25, 26}.

Recent studies converge toward a model
whereby talin may initially interact with
vinculin in a force-independent regime²⁷⁻³⁰
leading to partial relief of autoinhibition yet
how these force-independent complexes
transition into high affinity mechanical
linkages is not fully understood. High-
affinity vinculin binding to talin requires
exposure of the VBSs buried in the α -
helical bundles in the talin rod domains¹⁴⁻¹⁶.
³¹ Recent studies have revealed that
forces within the physiological range, in the
order of several piconewtons (pN), can fully
expose the cryptic VBSs in talin and enable
high-affinity vinculin D1 binding¹⁴⁻¹⁶. While
previous studies have shown that isolated
talin VBSs bind vinculin with dissociation
constants over a range of 70 - 500 nM³²,
which could activate vinculin binding to
actin filaments²⁹, it remains unclear how
mechanically exposed VBSs in the context
of unfolded rod domains might interact with

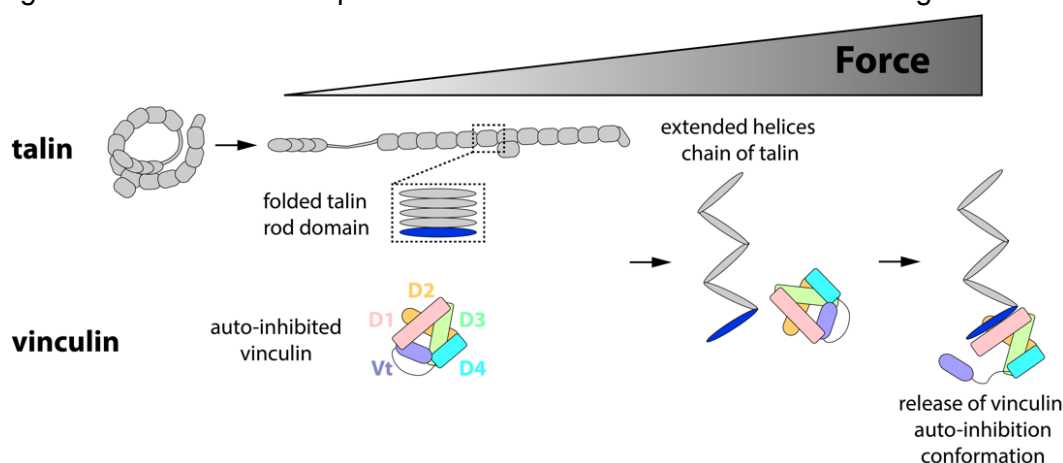


Figure 1. Schematic of the force-dependent vinculin activation by talin. In the absence of force, both the VBS (blue) in talin rod domains and FL-vinculin are autoinhibited. Force is needed to expose the VBS in talin rod domain by unfolding the α -helix bundle. The mechanically exposed VBS can bind to the D1 domain (pink) and compete off the tail, Vt, which releases the autoinhibitory conformation.

1
2
3 vinculin. In contrast to an isolated VBS,
4 which exists in a force-free environment,
5 the mechanically exposed VBS in talin are
6 under forces of several pN^{12, 13, 16}, which
7 may alter the conformation of the VBS
8 significantly impacting on the binding
9 affinity³³ and kinetics³⁴. Hence, further
10 studies on the force-dependent
11 conformations of VBSs under a few pN
12 forces and the resulting effects on the
13 vinculin-talin VBS interaction may provide
14 insight into this important linkage.
15
16
17
18
19

20 A further layer of regulation arises from the
21 fact that vinculin is also autoinhibited, and
22 in the absence of other factors, vinculin
23 adopts a compact globular conformation, in
24 which the vinculin head interacts with the
25 vinculin tail suppressing its interactions
26 with most of its binding partners (Fig. 1). As
27 vinculin head binds to its tail with high
28 affinity *in vitro*^{35, 36}, this autoinhibitory
29 interaction is thought to be strong. Several
30 models have been proposed to explain the
31 vinculin activation process at cell
32 adhesions. The widely accepted
33 combinatorial model proposes that at least
34 two binding partners are required to
35 associate with vinculin head and tail
36 simultaneously to overcome the strong
37 head-tail interaction^{23, 37}. However, based
38 on the high-affinity interaction between
39 vinculin D1 and isolated talin VBS, the
40 possibility of a single ligand activation
41 model cannot be excluded. Since the
42 vinculin-talin and vinculin autoinhibitory
43 associations are mutually exclusive, the
44 D1-VBS interaction may provide sufficient
45 energy to compete off Vt from D1^{32, 38, 39}. In
46 addition, the crystal structure of
47 autoinhibited vinculin shows that
48 autoinhibition is mediated by a number of
49 head-tail interactions, with the D1-Vt
50 interaction being the predominant
51 interaction. As such disruption of the D1-Vt
52 interaction by a talin VBS may destabilize
53
54
55
56
57
58
59
60

the whole head-Vt interaction, driving a
conformational change to a more extended
activated conformation³².

Another important facet of the dynamics of
these linkages is their lifetime. The talin-
mediated force-transmission
supramolecular linkages have an average
lifetime in the order of minutes⁴⁰ although a
significant population of talin is immobile in
focal adhesions⁴¹ and at muscle
attachment sites⁴². Therefore, the binding
of vinculin to talin in cells happens within a
limited time window. When talking about
the head-tail autoinhibition of vinculin, one
should consider whether such
autoinhibition can significantly suppress
the binding over this physiologically
relevant time scale. After binding to talin's
mechanically exposed VBSs, vinculin
mediates a cascade of downstream
biochemical events through interactions
with a plethora of cytoskeletal and signaling
proteins^{2, 3, 25, 26}. It is reasonable to believe
that the longer the activated vinculin is
associated with talin, the more persistent the
vinculin-mediated
mechanotransduction. Hence, the
information of the lifetime of vinculin bound
to talin under force is important but has not
been investigated in previous studies.

In this study, we show that FL-vinculin can
bind to a mechanically exposed talin VBS
in R6 at ~10 nM concentrations, much
lower than the dissociation constants
measured for isolated VBSs that are not
under force³². Molecular Dynamics (MD)
simulation on isolated VBS reveals a
propensity for the VBS helix to collapse into
a compact hairpin-like arrangement in the
absence of tensile force, which autoinhibits
the VBS but can be released by
physiological forces. The kinetics of the
interaction between vinculin and the
mechanically exposed VBS is

characterized with a fast association rate k_{on} in the order of $10^6 M^{-1} \cdot s^{-1}$, and a dissociation rate k_{off} in the order of $10^{-2} s^{-1}$. In addition, by comparing the results with those obtained from vinculin D1, the vinculin head, and a vinculin T12 mutant with a weaker autoinhibitory head-tail interaction, we determine the influence of inter-domain interactions within vinculin on the kinetics and affinity of the force-dependent vinculin-talin interaction.

Results

A force-jump cycle assay to quantitate vinculin-talin complexation at the single-molecule level

The interactions between the vinculin D1 domain and VBS-bearing talin, α -catenin and α -actinin domains have been extensively studied^{14-16, 43, 44}. In contrast,

relatively little is known about the force-dependent binding of FL-vinculin to these VBS-bearing mechanosensing proteins. In this study, we wanted to study binding of FL-vinculin to a well characterized mechanosensitive system, and we chose talin domains R4-R6 which contain three α -helical bundles and a single VBS buried in R6 (helix 27) (Fig. 2A-B). Talin R4-R6 was tethered between a glass surface and a superparamagnetic bead which enabled force to be exerted onto the domains (Fig. 2A).

To detect and quantify binding of FL-vinculin to mechanically unfolded R4-R6 we implemented a force-jump cycle approach (Fig. 2C). Each force-jump cycle

included the following steps: 1) a vinculin displacement step: the single-molecule construct was held at 50 ± 5 pN for 10 seconds to ensure displacement of any

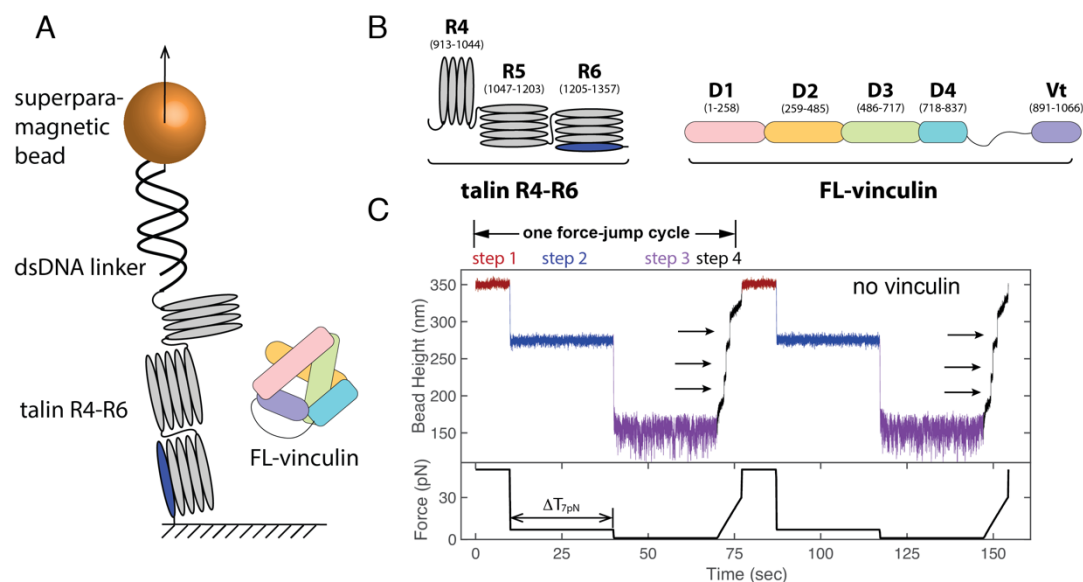


Figure 2. Force-jump cycle to detect and quantify vinculin binding. (A) Schematic of the talin R4-R6 domains tethered between a glass surface and a superparamagnetic bead. A 572-bp DNA linker is added as a spacer. (B) Domain map of talin R4-R6 (left) and FL-vinculin (right). The cryptic VBS in R6 is shown in blue. (C) Force-jump cycle applied to the talin R4-R6 domains in the absence of vinculin. Black arrows indicate the three discrete unfolding steps corresponding to R4-R6 domains. (bottom: the experimental time trace of force change).

bound vinculin within seconds with 100% probability¹⁶; 2) a vinculin binding step: force-jump to a vinculin-binding force of 7 ± 0.7 pN for a certain time interval, $\Delta T_{7\text{pN}}$ to allow vinculin binding to the mechanically exposed VBS; 3) a talin refolding step: force-jump to domain-folding force of 1 ± 0.1 pN for 30 seconds to allow all domains to refold with 100% probability unless vinculin remains bound to the VBS preventing refolding of R6¹⁶; and 4) binding detection step: force was increased from 1 ± 0.1 pN to 30 ± 3 pN at a loading rate of 4 ± 0.4 pN/s, during which all the domains unfold. After this step, force was jumped back to 50 ± 5 pN for the next vinculin displacement step, which completes one force cycle.

A vinculin-binding force of ~ 7 pN was chosen to detect the binding of vinculin to mechanically exposed VBS, because it lies within the physiological range of forces (5 – 12 pN) applied to talin in cells^{12, 16}. In addition, at this force, refolding has never been observed over a long time scale (> 400 seconds)¹⁶, which ensured that the VBS was always exposed for binding. At the domain-folding force of ~ 1 pN, in the absence of other factors, all talin rod domains fold almost immediately. In step 4 for the binding-detection, if no vinculin was bound then three unfolding events would be observed as seen in Fig. 2C. However, if a domain remains unfolded after 30 seconds, this can be attributed to vinculin-binding to the VBS preventing refolding of the VBS-containing R6 domain. Therefore, this assay enables us to monitor whether a vinculin molecule is bound to our talin molecule; if R6 is not able to refold in step 3 due to vinculin remaining bound, only two unfolding events from R4 and R5 would be observed indicating formation of a talin-vinculin complex.

The response of talin R4-R6 to cyclic force perturbation

Fig. 2C shows a representative time trace of more than 10 independent tethers of bead height change during a force-cycle in the absence of vinculin. At step 1 where the tether was held at 50 ± 5 pN, the bead height fluctuated around a constant average level of 350 nm (data shown in red). The following force-jump to 7 ± 0.7 pN resulted in a large abrupt height decrease to an average level of 274 nm (data shown in blue). The next force-jump to 1 ± 0.1 pN resulted in another abrupt height decrease to an average level of 151 nm (data shown in purple). During the subsequent force-increase scan from 1 ± 0.1 pN to 30 ± 3 pN (data shown in black), three unfolding steps were observed (black arrows), indicating full refolding of all the three domains when the construct was held at 1 ± 0.1 pN in this force-cycle. Here we note that the abrupt bead height changes during sudden large force jumps are contributed from both intrinsic molecular extension change, and bead rotation due to torque rebalance after the force change⁴⁵. In contrast, the stepwise bead height changes during force-increase scans represent molecular extension changes. This is because the force change before and after the steps are less than 0.04 pN, hence the torque remains balanced and therefore the bead rotation is negligible⁴⁵.

Vinculin binds to mechanically unfolded talin

Repeating the force-cycle in the presence of 10 nM FL-vinculin revealed only two unfolding events (indicated by black arrows) at the binding detection step in the first force-jump cycle (Fig. 3A) with $\Delta T_{7\text{pN}} = 30$ s. This indicates that one domain did not

refold at step 3 when the construct was held at 1 ± 0.1 pN for 30 seconds. Since the failure of the domain to refold was dependent on the presence of FL-vinculin, it was attributed to the vinculin-bound R6. In cycle 2, three unfolding steps were observed, indicating no vinculin was bound to the VBS in the vinculin binding step. The probability of having a FL-vinculin bound during any given cycle provides important information on the binding affinity of the interaction.

The fact that vinculin binding was observed in these experiments indicates that mechanical exposure of the VBS in R6 is sufficient for FL-vinculin binding at nM concentrations, suggesting that the autoinhibitory head-tail interaction of vinculin is not strong enough to suppress vinculin binding to a mechanically exposed VBS.

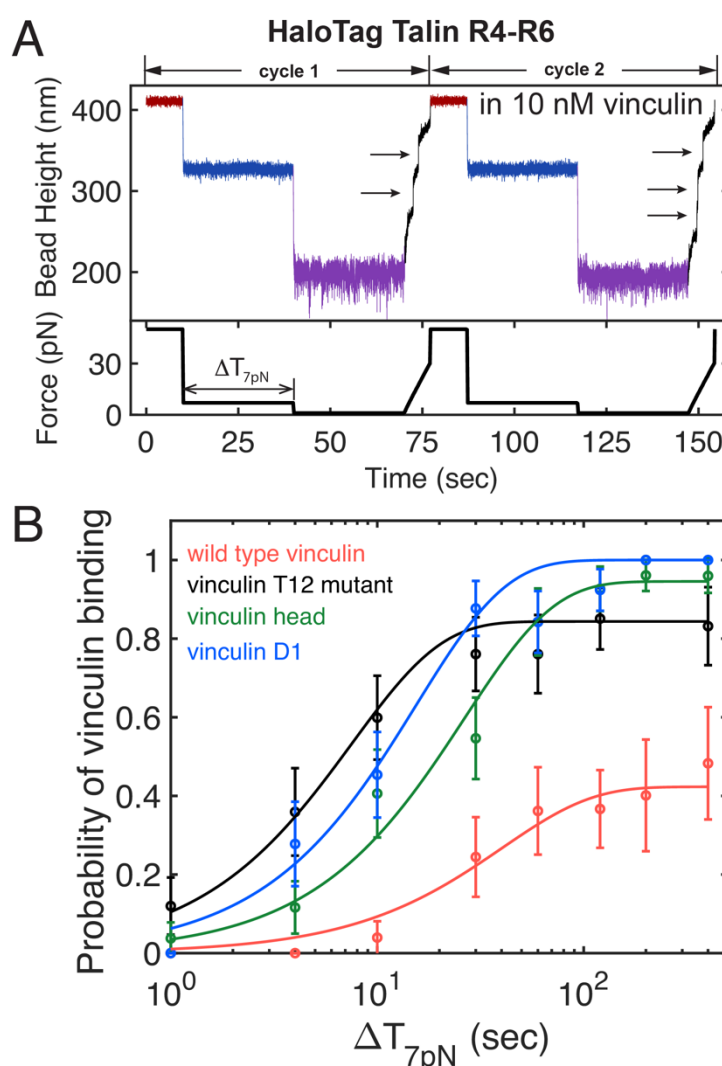


Figure 3. Full-length vinculin binds to mechanically exposed VBS in talin with nM affinity. (A) Representative force-jump cycles applied to detect and quantify vinculin binding. (B) The time evolution of binding probability for wild type vinculin (red), T12 mutant (black), vinculin head (D1-D4, green), and vinculin D1 (blue) are shown. The evolution for vinculin binding probability was taken at ΔT_{7pN} =1 s, 4 s, 10 s, 30 s, 60 s, 120 s, 200 s, and 400 s.

Quantification of vinculin binding to a mechanically exposed VBS

We next sought to quantify the interaction between talin and vinculin by determining the binding kinetics and affinity. To do this, we implemented the force-jump cycle (Fig. 2C) to obtain the probability of FL-vinculin binding to the mechanically exposed VBS in talin R6 at 7 ± 0.7 pN with different holding times $\Delta T_{7\text{pN}}$. At each $\Delta T_{7\text{pN}}$, the binding probability was determined by $\frac{N_b}{N}$, where $N \geq 15$ was the total force-cycles obtained from multiple tethers and N_b was the number of cycles where vinculin binding was observed. Repeating the force-cycle at different $\Delta T_{7\text{pN}}$, we determined the time evolution of the binding probability $P(t)$ of FL-vinculin binding to the mechanically exposed VBS in talin R6.

In Fig. 3B, the red data points show the probability of FL-vinculin binding to the mechanically exposed R6 VBS obtained at 10 nM FL-vinculin. Shown in red is the best-fit curve with $P(t) = \frac{ck_{on}}{ck_{on}+k_{off}} \left(1 - e^{-(ck_{on}+k_{off})t}\right)$, where c , k_{on} and k_{off} are vinculin concentration, association rate and dissociation rate, respectively. The best-fit parameters are determined to be $k_{on} = 1.0 \pm 0.4 \times 10^6 \text{ M}^{-1}\text{s}^{-1}$ and $k_{off} = 1.4 \pm 0.9 \times 10^{-2} \text{ s}^{-1}$, from which the dissociation constant was calculated to be $K_d = \frac{k_{off}}{k_{on}} = 12 \pm 5 \text{ nM}$. We note that, to accurately determine the rate constants, it is important to choose $\Delta T_{7\text{pN}}$ that covers both non-equilibrium and equilibrium regimes (Supp. Info. 1). The result indicates that FL-vinculin can directly bind to the mechanically exposed VBS in talin R6 with nM affinity. The standard error was calculated as the standard deviation of means based on bootstrap analysis with

200 repetitions (See Methods). The association rate is in the order of diffusion limited on-rate⁴⁶; hence, the result strongly suggests that the FL-vinculin undergoes a highly dynamic fluctuation between the auto-inhibited closed conformation and an open conformation accessible to the VBS.

Quantification of vinculin T12 mutant, vinculin head and vinculin D1 binding to mechanically exposed VBS

Having established that FL-vinculin binds to mechanically exposed VBS in talin, we next characterized the interaction in more detail using a series of well-established vinculin constructs. These included the “vinculin T12” mutant that has reduced autoinhibition due to weaker head-tail interaction³⁵, the entire vinculin head (D1-D4), and the VBS-binding domain of vinculin (D1) which is expected to bind talin with maximal affinity. Similar binding experiments were performed for each of these vinculin constructs to enable direct comparison with FL-vinculin (Fig. 3B).

Vinculin T12 mutant - The vinculin T12 mutant contains four mutated residues in the vinculin tail domain, Vt (D974A, K975A, R976A and R978A)³⁵. Previous experiments have shown that the T12 mutant has a weaker head-tail interaction due to disruption of the D4-Vt interface, resulting in stronger binding to talin and enhanced focal adhesion formation and stabilization³⁵. In our force-cycle experiments, 10 nM vinculin T12 (Fig. 3B, black curve) bound to the mechanically exposed VBS in talin R4-R6 with the following best-fitting values, $k_{on} = 1.1 \pm 0.3 \times 10^7 \text{ M}^{-1}\text{s}^{-1}$ and $k_{off} = 2.1 \pm 1.1 \times 10^{-2} \text{ s}^{-1}$. The dissociation constant was calculated to be $K_d = 1.9 \pm 0.5 \text{ nM}$. Compared to wild type vinculin, T12 has a significantly faster association rate but a

similar dissociation rate, resulting in a higher binding affinity indicated by a ~6-fold lower dissociation constant.

Vinculin head - The vinculin head comprises D1, D2, D3 and D4 domains that show extensive interdomain interactions, although the construct lacks the autoinhibitory Vt domain. Similar experiments performed in 10 nM vinculin head (Fig. 3B, green curve) gave best-fitting values of $k_{on} = 3.7 \pm 0.9 \times 10^6 M^{-1}s^{-1}$ and $k_{off} = 2.2 \pm 1.8 \times 10^{-3} s^{-1}$. The dissociation constant was calculated to be $K_d = 0.6 \pm 0.3$ nM. The measured value of k_{off} is in good agreement with that reported from a previous Fluorescence Recovery After Photobleaching (FRAP) measurement¹⁹.

Vinculin D1- Similar experiments with the vinculin D1 alone (Fig. 3B, blue curve) determined a best-fitting value of $k_{on} = 6.5 \pm 1.6 \times 10^6 M^{-1}s^{-1}$ and a near-zero k_{off} which cannot be accurately determined by fitting, due to ~1 equilibrium binding probability $P_{eq} = \frac{ck_{on}}{ck_{on}+k_{off}}$ measured in our experiments. Together, these results suggest a much higher

binding affinity for vinculin D1, which cannot be determined within our experimental time scale, than that of the vinculin head, FL-vinculin and the T12 vinculin mutant.

The best-fitting values of k_{on} and k_{off} and the resulting K_d are summarized in Table 1. These results suggest that although all four forms of vinculin can bind the mechanically exposed VBS at nM concentrations, the binding affinity is the highest for D1 ($K_d < 1$ nM, Supp. Info 4) and the weakest for FL-vinculin. The dissociation rates for the FL-vinculin and the T12 mutant are similar; therefore, the increased affinity of T12 is mainly caused by a near 10-fold faster association rate compared to the wild type vinculin. This suggests that the dynamic head-tail interaction within the wild type vinculin reduces the time fraction of the open, accessible conformation. In contrast, the weaker head-tail interaction in T12 leads to a higher propensity to exist in a more accessible conformation, which is in line with a recent study reporting less energy is needed to shift from a closed to a semi-open state of T12 than that of wild type vinculin⁴⁷.

Table 1. Kinetic rates and affinity of vinculin binding to mechanically exposed VBS

	FL-vinculin	T12 vinculin	vinculin head	vinculin D1
$k_{on} (M^{-1}s^{-1})$	$1.0 \pm 0.4 \times 10^6$	$1.1 \pm 0.3 \times 10^7$	$3.7 \pm 0.9 \times 10^6$	$6.5 \pm 1.6 \times 10^6$
$k_{off} (s^{-1})$	$1.4 \pm 0.9 \times 10^{-2}$	$2.1 \pm 1.1 \times 10^{-2}$	$2.2 \pm 1.8 \times 10^{-3}$	Too low to be detectable
K_d (nM)	12 ± 5	1.9 ± 0.5	0.6 ± 0.3	Not available

The association rates of vinculin head and D1 are faster than that of the FL-vinculin by several folds. In addition, their dissociation rates are ~ 6 -fold (for vinculin head) and much more (for vinculin D1) slower than that of the FL-vinculin. Together, the faster association rates and slower dissociation rates result in the higher affinity of vinculin head and D1 than that of the FL-vinculin.

Overall, these results reveal important differences between the binding of the four forms of vinculin to talin VBS. The most important is that, while the head-tail interaction of vinculin does not inhibit vinculin binding to mechanically exposed VBS, it significantly tunes the affinity mainly via modulating the rates of binding.

The force-dependent conformations of an exposed talin VBS tune its affinity for vinculin

A striking finding of our study is that the affinity of the talin-vinculin interaction observed under force is significantly higher than the bulk interactions of talin VBS with FL-vinculin measured in solution (70 - 500 nM)³². As, the mechanically exposed VBS have enhanced binding affinity relative to isolated VBS in solution, it suggests that forces applied to a talin VBS strongly influence binding to vinculin. The talin-vinculin interaction involves the VBS binding as a helix to the D1 domain via a helix-addition mode of binding (illustrated in Supp. Fig. 3A). In the folded talin rod domain, a VBS also adopts a helical conformation as part of the helical bundle.

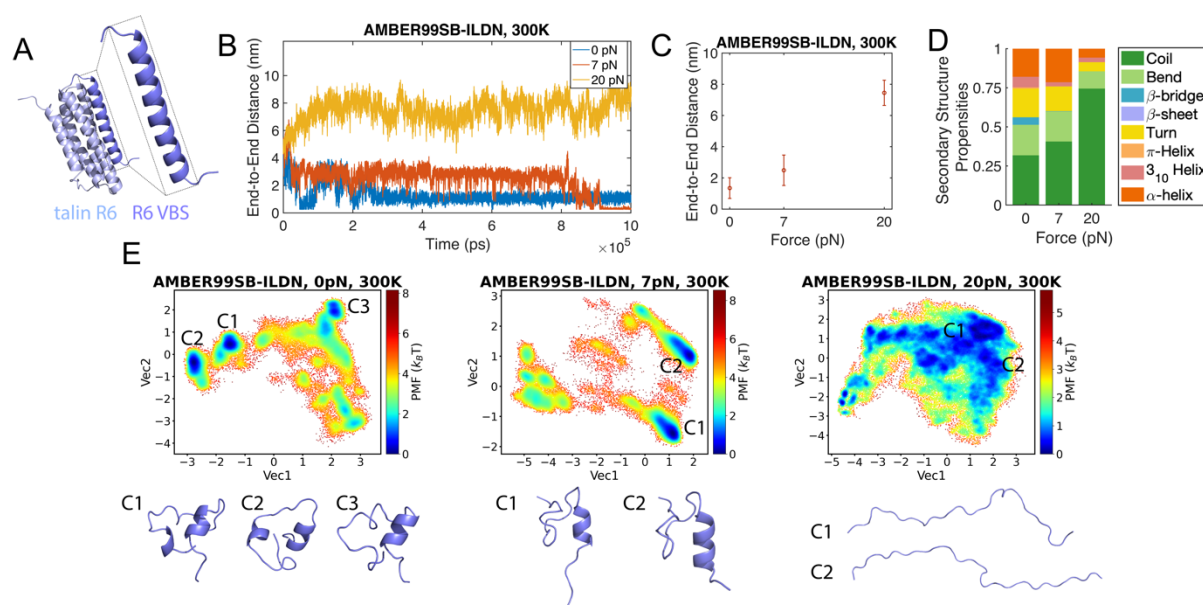


Figure 4. Force-dependent conformations of the talin R6 VBS. (A) Solution structure of talin R6 domain (PDB 2I10). The inset shows the α -helical conformation of the R6 VBS used as the initial conformation. (B) Time traces of the end-to-end distance of R6 VBS under different tensile forces using AMBER99SB-ILDN force field at 300K. (C) The mean and standard deviation of the end-to-end distance of R6 VBS calculated from the time traces at 300K using AMBER99SB-ILDN force field. (D) Secondary structure propensities of R6 VBS under different tensile forces using AMBER99SB-ILDN force field at 300K defined by DSSP. (E) Free energy landscape as a function of the first two dihedral principal components using AMBER99SB-ILDN force field at 300K at 0, 7, and 20 pN, with the representative conformations of identified local energy minima.

1
2
3 However, an exposed VBS, which is not
4 bound to vinculin, has the potential to adopt
5 various conformations besides the high
6 affinity vinculin-binding helical form.
7 Hence, we hypothesized that the isolated
8 VBS may adopt thermodynamically stable
9 autoinhibited conformations that
10 suppresses its binding to vinculin D1. To
11 evaluate the potential effect of force on
12 VBS conformation we performed 1- μ s full-
13 atom molecular dynamics (MD) simulations
14 on a VBS peptide with and without applied
15 forces. The α -helical conformation
16 obtained from the folded R6 domain
17 structure (PDB 2110³¹), was used as the
18 initial VBS conformation in the simulations
19 (Fig. 4A).

20
21 Simulations were performed on the R6
22 VBS by itself in 150 mM NaCl solution
23 starting from the initial α -helical
24 conformation up to 1 μ s under
25 AMBER99SB-ILDN⁴⁸ force field, at
26 temperature of 300K (See Methods). The
27 time traces of the end-to-end distance of
28 R6 VBS show significant dependence on
29 the applied force (Fig. 4B). In the absence
30 of force, the end-to-end distance collapsed
31 from the initial value (\sim 4.1 nm) of the helical
32 conformation to \sim 1.0 nm after 200 ns of
33 simulation and remained in the compact
34 conformation throughout the rest of
35 simulation. At 7 pN, the VBS assumed
36 overall more extended conformations and
37 larger extension fluctuations. At 20 pN, the
38 end-to-end distance evolved from the initial
39 value to a larger value (\sim 8.4 nm), indicating
40 transition to conformations that are more
41 extended than the original helical
42 conformation. Consistently, the average
43 extension of R6 VBS monotonically
44 increases as the applied force increases
45 (Fig. 4C). Together, the results reveal that
46 forces in physiological range strongly
47 modulate the conformations and the
48 extension of a VBS. It is likely that all

exposed talin helices exhibit similar force-
dependent conformational changes.
Indeed, similar results were obtained from
another talin, the VBS in R10, VBS3 (Supp.
Info. 3).

To obtain information on the predominant
conformations at each force, we performed
the dihedral principal component analysis
(dPCA)⁴⁹ and used the first two principal
component axes to recast the simulation
data (See Methods). Fig. 4E shows the free
energy landscape of R6 VBS as a function
of the first two dihedral principal
components of the 1- μ s MD simulation in
the absence of force, as well as at forces of
7 and 20 pN at 300K using AMBER99SB-
ILDN force field, and a few representative
predominant snapshots of conformations
identified by dPCA at each force. At 0 pN,
the free energy landscape represents
multiple local energy minima and the
corresponding R6 VBS conformations all
exhibit compact hairpin-like structures.
The 20 lowest energy structures of the R6
VBS, aligned on the first helical segment
(residues 1330-1336) (Supp. Info. 2),
illustrates that the collapsed state is only
partially ordered and has conformational
heterogeneity rather than a single low
energy folded state. The NMR spectrum of
the R6 VBS (Supp. Info. 2) supports this
assessment as the lack of dispersion and
relative broadness of the peaks is
indicative of a peptide with some transient
structural features but conformational
heterogeneity. At 7 pN, the predominant
conformations of the R6 VBS peptide
becomes a mixture of helical and
disordered regions. At 20 pN, the R6 VBS
exists predominantly as a disordered,
extended peptide. Fig. 4D summarizes the
amino acid secondary structure propensity
in 1- μ s MD simulation at different forces
determined by the Dictionary of Protein
Secondary Structure (DSSP) algorithm⁵⁰.

Similar results were also obtained from VBS in R10 (Supp. Info. 3).

Together, the simulations suggest that the conformation of an isolated talin VBS is very sensitive to the force applied over a physiological range. Interestingly, in the absence of forces, an isolated VBS has the propensity to collapse into energetically favorable hairpin-like conformations that not only drastically deform from the original α -helical conformation but also bury several critical residues that mediate the interaction with vinculin D1. This compact form is likely to be a previously unrecognized, autoinhibited conformation

that binds D1 with reduced affinity. In addition, at too large a force (e.g., 20 pN), a VBS becomes a completely disordered peptide. At the physiologically relevant forces of a few pN such as 7 pN, a VBS is a dynamic mixture of helical and disordered regions which is expected to enhance binding to D1 compared with the collapsed hairpin-like conformations in the absence of force or the completely disordered peptide conformation at large forces > 20 pN. Consistent with this picture, the dissociation constant between isolated R6 VBS (helix 27) and vinculin D1 was determined to be 320 ± 30 nM using fluorescence polarization assay (Supp. Info.

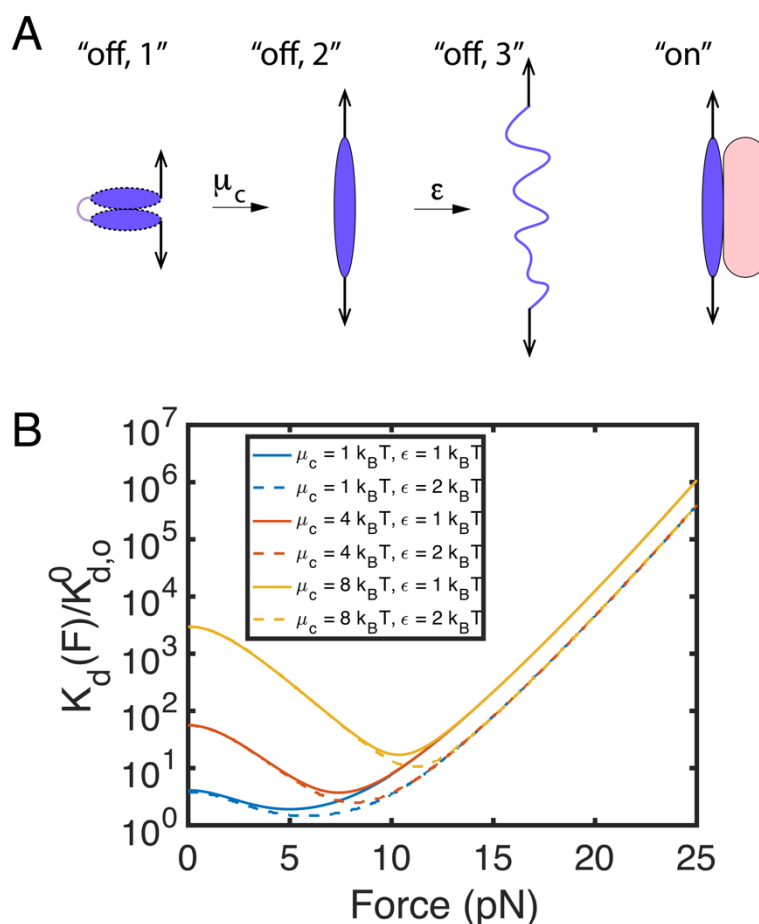


Figure 5. Force-dependency of the VBS conformation and its interaction with vinculin D1. (A) Schematic of four states of an isolated VBS, three unbound, “off” states, and the vinculin D1 bound “on” state. The pink rounded rectangle represents vinculin D1 which binds to the helical “on” conformation. (B) Fold change in the force-dependent binding constant, $K_d(F)$ of the VBS-D1 interaction (Eq. 1), maximal binding affinity is seen in the trough of the curve at 5-11 pN dependent on the value of μ_c and ϵ .

4), which is orders of magnitude larger than that between mechanically stretched R6 VBS and vinculin D1. As further validation of this enhanced binding affinity of a VBS under force compared to an isolated VBS we find that micromolar concentrations of isolated R6 VBS are required to inhibit vinculin D1 binding to a mechanically stretched R6 VBS (Supp. Info. 4).

Based on the insights provided from the MD simulations, we developed a simple model to understand the force-dependent binding affinity between an isolated talin VBS and the VBS binding D1 domain in vinculin. In this model, three structural states of the VBS are considered (Fig. 5A): the α -helical conformation that binds D1 with the highest affinity (state "off, 2"), an autoinhibited hairpin-like conformation (state "off, 1") and a disordered peptide conformation that does not bind D1 (state "off, 3"). Besides the three "off" states of VBS unbound by D1, a fourth state where the VBS is bound to D1 (state "on") exists. Based on these four states, we derived a force-dependent dissociation constant of the VBS-D1 interaction as:

$$K_d(F) = K_d^0 \left(1 + e^{\beta\mu_c} e^{-\beta\Delta\phi_{1,2}(F)} + e^{-\beta\varepsilon} e^{-\beta\Delta\phi_{3,2}(F)} \right). \quad (1)$$

where $\beta = \frac{1}{k_B T}$. K_d^0 denotes the dissociation constant of the original α -helical conformation of VBS binding to D1 in the absence of force. μ_c is the autoinhibitory free energy stored in an ensemble of hairpin-like conformations, which is the free energy difference between the original α -helical conformation and the hairpin-like conformations. ε is the free energy difference between the ensemble of unstructured peptide conformation and α -helical conformation of VBS. The value of ε tunes the probabilities of the α -helical

conformation and the unstructured peptide conformations, which can be roughly understood as the stability of the α -helical conformation of the VBS. $\Delta\phi_{1,2}(F)$ is the force-induced conformational free energy difference between the "off, 1" and "off, 2" states, and similarly $\Delta\phi_{3,2}(F)$ is the force-induced conformational free energy difference between the "off, 3" and "off, 2" states. These force-induced conformational free energy differences can be calculated based on the different force-extension curves of the corresponding structural states i and j , $\Delta\phi_{i,j}(F) = -\int_0^F (x_i(f) - x_j(f)) df$, where $x_i(f)$ is the force-extension curve of the conformation state "off, i ". Details of the general physics behind the derivation can be found in our recent publication³³, and the calculation for this particular case is provided in the supplementary information (Supp. Info. 1).

Fig. 5B shows predicted K_d relative to K_d^0 for the VBS binding to the vinculin D1 as a function of force applied to the VBS (Eq. 1). As shown, with a reasonable assumption of $k_B T$ level of the autoinhibition energy of μ_c in the hairpin-like structure, the equation predicts that forces of a few pN would significantly increase the binding affinity which sensitively depends on the level of autoinhibition energy stored in the hairpin-like conformations. Furthermore, the force dependent binding constant, has maximal affinity (the trough on the curves in Fig. 5B), that is determined by the stability of the VBS helix, as such helix stability further tunes the talin-vinculin interactions. As a result, further complexity and nuance is added to the talin-vinculin interactions, as even at the level of an exposed VBS the affinity between a VBS helix and vinculin is dynamically regulated by mechanical forces.

Discussion

The interplay between talin and vinculin dictates mechanotransduction pathways downstream of integrins. A remarkable aspect of the interactions between these two proteins is its complexity. Both talin and vinculin adopt autoinhibited states, and once activated, the lifetimes of their association are largely defined by the mechanical conditions of the system and the history of prior forces that have acted on the linkages. In this study, we investigated the interaction between autoinhibited vinculin and talin, by using a three domain talin construct, R4-R6 that contains a single cryptic VBS in R6. Strikingly, these two proteins do not interact in the absence of force, but mechanical exposure of the VBS in R6 is sufficient for binding to autoinhibited vinculin, revealing that force applied to talin alone is sufficient to activate high-affinity binding of vinculin in the absence of other factors. Furthermore, we identify an additional layer of regulation whereby the affinity of an exposed VBS for vinculin is fine-tuned by force-dependent changes in the conformation of the VBS helix itself. Steered full-atom molecular dynamics simulation reveals that a VBS peptide can adopt an autoinhibited stable hairpin-like conformation, which can be unfurled at physiological ranges of force. We reason that force may release the autoinhibited hairpin-like conformation of the VBS enhancing its affinity for vinculin.

Autoinhibition of proteins involved in cell adhesion represents a major mechanism encoding mechanosensitivity⁵¹ and enabling force-dependent binding constants³³. Full-length talin and vinculin are both regulated by autoinhibition^{23, 24, 52, 53}, and a recent study by Atherton et al. using a mitochondrial targeting assay

showed that the two autoinhibited proteins do not interact²⁷. Release of the autoinhibition of either of the proteins led to their association in a force-independent manner. In the same study²⁷, talin null cells co-expressing full-length vinculin and full-length talin under tension-released condition only formed small peripheral adhesions. Activation of either protein via mutagenesis was shown to be sufficient to enable their co-localization in focal adhesions under the condition where the actomyosin cytoskeleton contraction was suppressed using blebbistatin. However, the affinity of such force-independent association between talin and vinculin could be significantly weaker than that when VBSs in talin are mechanically exposed. Indeed, in the same study the authors showed that actomyosin contraction was needed for full maturation of focal adhesion. Similar force-independent talin-vinculin interactions have been proposed previously by Han et al. via a weak talin R8 – vinculin D1 interaction³⁰ indicated by a dissociation constant in the order of μM range⁵⁴. Such force-independent pre-complexation between talin and vinculin was shown to be required for efficient adhesion maturation. The presence of phosphoinositides at the membrane have also been shown to be able to activate talin and enable force-independent interactions with vinculin²⁸. Here, we show that full-length vinculin can bind to the mechanically exposed VBS in talin R6 with nM affinity, indicating that mechanical activation of talin is sufficient to trigger high-affinity binding to full-length vinculin. Together, these results highlight the cascade of activation steps that ultimately lead to the interactions between these two proteins. It is likely that there are multiple diverse pathways and mechanisms that can bring talin and

1
2
3 vinculin together prior to tension and the
4 assembly of mechanical linkages.
5
6

7 Binding of vinculin to a mechanically
8 exposed talin VBS is fast with an
9 association rate of $\sim 10^6 \text{ M}^{-1}\text{s}^{-1}$, close to
10 the typical diffusion limited association
11 rate⁴⁶. This is surprising, since vinculin was
12 thought to adopt a strongly autoinhibited
13 closed conformation due to the Vt-D1
14 interaction^{23, 24, 35}. The fast association rate
15 observed in our experiment strongly
16 suggests that the autoinhibitory Vt-D1
17 interaction does not significantly slow down
18 the binding of vinculin to a mechanically
19 exposed talin VBS. Therefore, we propose
20 that vinculin must undergo spontaneous
21 rapid dynamic fluctuation between the
22 open and closed states, making the
23 vinculin D1 domain accessible for rapid
24 binding to a talin VBS.
25
26
27
28
29

30 31 Force-independent talin-vinculin 32 interactions enhance the association 33 rate 34 35

36 An unexpected finding of this work is that
37 the vinculin T12 mutant, has the fastest
38 association rate of all of the vinculin
39 constructs tested. The vinculin D1 domain
40 interacts with the mechanically exposed
41 VBS with an association rate of $6.5 \pm$
42 $1.6 \times 10^6 \text{ M}^{-1}\text{s}^{-1}$, which is faster than that
43 of the entire vinculin head (D1-D4 domains)
44 or wild type vinculin, but slightly slower than
45 the T12 mutant. It is surprising that T12
46 binds the exposed VBS with a rate faster
47 than either D1 or head, as neither of them
48 contain the autoinhibitory Vt domain. We
49 therefore expected that binding of
50 constructs lacking Vt would be faster than
51 both the wild type vinculin and the T12
52 mutant. One possible explanation for this
53 result is that the Vt domain and/or the
54 preceding linker region might make some
55 form of non-specific interactions with the
56
57
58
59
60

unfolded talin domains. Unfolded talin rod
domains expose a lot of hydrophobic
sidechains, and the helical propensity and
hydrogen bond forming tendency of these
exposed sequences, means such non-
specific interactions are quite possible.
Such non-specific interactions would
increase the effective local concentration of
vinculin, promoting a fast binding rate of the
vinculin D1 domain in the T12 mutant to the
VBS. The Vt domain and the linker may
therefore mediate pre-complexation of FL-
vinculin with partially exposed VBS-
containing sites prior to canonical VBS-D1
engagement. This interaction would
accelerate binding to the VBS once it is
mechanically exposed.

It is also interesting to note that the
equilibrium binding probability of vinculin
D1 domain to the mechanically exposed R6
VBS reached ~ 1 in 10 nM of vinculin D1,
suggesting an ultra-slow dissociation rate
that could not be quantified in our assay.
The dissociation rate of the head was about
6-fold and 10-fold slower than that of the
wild type vinculin and the vinculin T12
mutant, respectively. Therefore, compared
with the wild type vinculin and the T12
mutant, the D1 and head domains have the
highest affinity mainly due to their slower
dissociation rate. This high affinity of D1
locks talin in an unfolded conformation¹⁵
and expression of vinculin D1 in cells leads
to loss of adhesion dynamics^{11, 55} and
lethality in flies⁵⁶. Although the vinculin
head-tail interaction is insufficient to inhibit
vinculin binding to a mechanically exposed
talin VBS, our results reveal that it
significantly tunes the affinity and binding
rates between vinculin and VBS. The T12
mutant with weakened head-tail interaction
binds VBS with an affinity 6-fold higher
compared to the wild type vinculin,
suggesting that the head-tail interaction
suppresses the binding of vinculin to a talin

1
2
3 VBS. Previous work has identified that
4 phosphorylation of vinculin, including at
5 Y100 and Y1605 by Src kinases, can
6 stabilize the open state^{57, 58}. Whilst our
7 data show that stretching talin alone is
8 sufficient to activate vinculin,
9 phosphorylation of these sites would
10 stabilize the open conformation of vinculin
11 extending the lifetimes of these mechanical
12 linkages.
13
14
15

16
17 In this scenario, the master switch for both
18 talin binding to vinculin and for vinculin
19 activation is the mechanical unfolding of
20 talin rod domains. Thus, we conclude that
21 talin is the mechanical switch for
22 talin/vinculin-dependent
23 mechanotransduction. Consistently,
24 previous studies have revealed that
25 talin/vinculin-dependent focal adhesion
26 development and maturation require
27 sufficiently rigid substrate⁵⁹, on which talin
28 is expected to experience considerable
29 mechanical stretching. In addition, earlier
30 work shows that applying external force to
31 focal adhesion sites results in increased
32 recruitment of vinculin to the perturbed
33 sites⁶⁰. These previous results are
34 consistent with the talin mechanical switch
35 model.
36
37
38
39
40
41

42 Identification of an additional layer of 43 talin autoinhibition

44 Talin is regulated by many layers of
45 autoinhibition⁶¹, from the fully closed form
46 in the cytosol which, upon relief of this
47 head-tail autoinhibition, can open up to
48 reveal the linear arrangement of helical
49 bundles. These bundles are autoinhibited
50 with respect to vinculin binding as they
51 contain cryptic VBS within the bundles
52 themselves. At physiological levels of
53 stretching e.g. 5-15 pN talin bundles unfold,
54 exposing the previously cryptic VBS, a well
55 characterized major mechanosensitive
56
57
58
59
60

event^{15, 16}. These domains remain unfolded
even when the force is reduced to just a few
pN, providing them with a mechanical
memory¹⁶. Here we define an additional,
previously unrecognized, layer of
autoinhibition on talin, at the level of the
individual VBS. Our MD simulations, and
the enhanced affinity for a VBS under force,
suggest that forces over a few pN range
increase the binding affinity by suppressing
the VBS from adopting a low affinity,
hairpin-like conformation. This provides an
explanation for the higher binding affinity
quantified in our single-molecule
experiments, where the VBS is under ~7
pN forces (Table 1), compared with that
from bulk measurement where the VBS is
not under force³². Similarly, the dissociation
constant between isolated R6 VBS and
vinculin D1 was found to be about two
orders of magnitude larger than that
between mechanically stretched R6 VBS
and vinculin D1 (Supp. Info. 4). We note
that mechanically exposed talin VBSs in
live cells are under similar level of tensile
forces^{12, 13}. Further increases in force on a
VBS reduce its binding affinity for vinculin
by decreasing the α -helical fraction of the
VBS¹⁵. Therefore, forces biphasically tune
the binding affinity of the exposed VBSs for
vinculin. This changing binding affinity as
forces on talin fluctuate means that the
affinity for vinculin is dynamically tuned,
even for an exposed VBS. Due to all these
modulators, the force-dependent
interactions of even a single VBS with
vinculin are complex, and talin has 11
VBSs.

Identification of an additional layer of vinculin autoinhibition

One intriguing finding of this work is that D1
binds faster and more tightly to an exposed
VBS than the vinculin head, which
suggests that the inter-domain interactions

1
2
3 within the vinculin head suppress vinculin
4 binding to talin. This raises the possibility of
5 an additional layer of vinculin autoinhibition
6 whereby the D1-VBS interaction is
7 hindered by the other head domains,
8 slowing down the binding rate compared to
9 D1 alone. As vinculin also makes a
10 mechanical linkage when it crosslinks talin
11 to actin, it too will experience mechanical
12 forces acting on it, and these forces,
13 exerted only when vinculin forms a
14 mechanical linkage, will extend vinculin. It
15 is possible that the inter-domain
16 interactions in the vinculin head can be
17 released by force-dependent changes in
18 the conformation of the head enhancing
19 talin binding. Such a scenario would
20 explain our data here, and if this is the case
21 it would suggest that the stability of vinculin
22 bound on talin might also be modulated by
23 force, this time acting on vinculin. Future
24 studies should investigate the effects of
25 forces exerted on vinculin binding to an
26 exposed VBS to confirm this layer of
27 autoinhibition of the talin-vinculin and how
28 force on vinculin modulates its affinity for
29 talin.
30
31
32
33
34
35
36
37
38

39 Talin-vinculin complexes as a way to 40 encode mechanical memory

41 In this study we have focused on the talin
42 module R4-R6 that contains a single VBS
43 in order to work with a simplified system,
44 and we show that force on talin drives talin-
45 vinculin complex formation. Complexation
46 stabilizes the open conformations of the
47 domains and thus alter the lifetimes of the
48 active conformations. Further, stabilization
49 of such interactions in vivo will occur when
50 the vinculin tail engages an actin filament³⁷,
51 which both stabilizes the open
52 conformation of vinculin and increases the
53 mechanical linkages on that integrin-talin-
54 actin connection. In a cell, there is the
55 opportunity for incredible diversity and
56
57
58
59
60

complexity in these mechanical linkages
based on the mechanical responses we
have identified. Each adhesive structure
contains many talin molecules⁶² each of
which contains 13 rod domains³¹. The 13
rod domains of talin can be envisaged as
binary switches with two states, folded “0”
and unfolded “1” and can be converted
between these states by changes in
mechanical force¹⁶. Within 9 of the talin rod
domains reside 11 VBSs, each of which
can be exposed by mechanical force to
bind vinculin. Therefore, just considering
the interaction between vinculin and talin
alone, the complexity of the mechanical
linkages that can form is staggering.
Further complexity emerges with the
discovery that the talin switches can be
modulated by post-translational
modifications such as phosphorylation
altering their mechanical response⁶³. It
is possible that other enzymes may also
modify the talin switches in response to
signaling, altering the mechanical
information stored in these linkages and
the resulting signaling hubs that
assemble¹⁸. The patterns of 1s and 0s in
each talin molecule will be stabilized by
vinculin binding to give persistent
mechanical linkages, and the effect of
future forces on the mechanical linkages
will result in additional exposure of VBSs in
other domains, explicitly dependent on the
talin-vinculin complexes already present.
This provides a basis for these mechanical
linkages to exhibit mechanical memory as
recently described in the MeshCODE
theory⁶⁴ with information stored in the
shape of these molecules and the
cytoskeletal connections that form as a
result.

Conclusions

In summary, we provide a comprehensive analysis of the complex interactions between full-length vinculin and a mechanically exposed VBS in talin, defining the fundamental mechanisms that regulate such interactions. In doing so we further expand our understanding of these crucial linkages that control mechanotransduction downstream of integrins.

Methods

Protein expression and purification

All plasmids were expressed in *Escherichia coli* BL21(DE3) cultured in Luria-Bertani (LB) media. The stretchable talin R4-R6 fragment was expressed and purified as reported previously¹⁶. Briefly, the expressed protein was purified via the GST-tag, using glutathione Sepharose resin (GE Healthcare) before being eluted by TEV cleavage. The FL-vinculin and vinculin T12 mutant plasmid constructs were synthesized by GeneArt gene synthesis and cloned into an expression vector (pET-28b). The vinculin head and vinculin D1 were cloned into pET-151 expression vector. The his-tagged vinculin proteins were purified through the his-tag followed by anion exchange using standard protocols⁶⁵. Protein concentrations were determined using the respective extinction coefficients at 280 nm.

Single-molecule manipulation

An in house-made back-scattered vertical magnetic tweezers was used in the single-molecule manipulation experiments with a spatial resolution of ~ 1 nm and temporal resolution of ~ 200 Hz^{45, 66}. Talin R4-R6 domains was tethered to the coverslip

through its C-terminal HaloTag/ligand system, while its N-terminus was linked to a superparamagnetic bead through a 572-bp double strand DNA linker. This system was performed in a laminar flow channel. The extension change of the tethered protein was measured based on the height change of the superparamagnetic beads tethered to the protein under force.

The details of the force calibration and control for the single-molecule magnetic tweezers experiments have been described in previous papers^{45, 66}.

Determination of k_{on} , k_{off} , K_d and error estimation

The binding kinetics involve the association and dissociation of binding which are characterized by the association rate k_{on} and the dissociation rate k_{off} , respectively. Denoting P as the probability of the VBS in the unfolded talin R6 bound by vinculin, it satisfies the equation: $\frac{dP}{dt} = ck_{on}(1 - P) - k_{off}P$, where c represents the vinculin concentration. With the well-controlled initial condition $P(0) = 0$, which refers to the assured unbound condition of talin R6 VBS at the starting point of step 2 (Fig. 2C), the equation can be solved as $P(t) = \frac{ck_{on}}{ck_{on} + k_{off}} \left(1 - e^{-(ck_{on} + k_{off})t} \right)$.

By implementing the force-jump cycles, the cycles with vinculin binding and those without vinculin binding at the vinculin-binding force (7 pN) can be recorded. At each time interval at 7 pN, $\Delta T_{7\text{pN}}$, an array A comprising N elements of 0 or 1 was generated, where $N \geq 15$ is the total number of cycles from multiple independent tethers. Elements of "0" and "1" indicate the cycles where the VBS was "unbound" and "bound", respectively. In our experiments, the force cycles were

performed at the following time intervals $\Delta T_{7pN} = 1$ s, 4 s, 10 s, 30 s, 60 s, 120 s, 200 s, 400 s.

After that, bootstrap analysis was performed for 200 repetitions to estimate the mean and the error of the fitted rates. Each bootstrap analysis randomly chooses N data points from the array A with replacement⁶⁷ and calculated the mean value of the N randomly selected data points, which is probability of binding $P_i(\Delta T_{7pN})$, at each ΔT_{7pN} , where $i = 1, \dots, 200$ refers to the i^{th} bootstrap analysis. For each bootstrap analysis, the resulting $P_i(\Delta T_{7pN})$ was fitted with the function of $P_i(\Delta T_{7pN}) = \frac{ck_{on,i}}{ck_{on,i} + k_{off,i}} \left(1 - e^{-(ck_{on,i} + k_{off,i})\Delta T_{7pN}} \right)$, from which the best-fitting values of $k_{on,i}$ and $k_{off,i}$ were obtained. Based on the fitted values of association rate $k_{on,i}$ and dissociation rate $k_{off,i}$, the dissociation constant $K_{d,i}$ can thus be determined by $K_{d,i} = \frac{k_{off,i}}{k_{on,i}}$. Upon completion of 200-repetition bootstrap (i.e., i was taken from 1 to 200), the mean values of the association rate k_{on} , dissociation rate k_{off} , and dissociation constant K_d were determined as the average over all $k_{on,i}$, $k_{off,i}$, and $K_{d,i}$, respectively. The standard error associated with k_{on} , k_{off} , and K_d were determined as the standard deviations of $k_{on,i}$, $k_{off,i}$, and $K_{d,i}$, respectively.

Molecular dynamics (MD) simulation

The MD simulation was performed using GROMACS 2020.2^{68, 69}. The initial talin VBS structures were R6 VBS (PASPNLKSQLAAAARAVTDSINQLITMC TQQA) structure taken from the NMR structure of talin R6 domain (PDB 2110³¹) and R10 VBS (YTKKELIESARKVSEKVVSHVLAALQA)

structure taken from the X-ray structure of the R10 VBS-human vinculin D1 complex (PDB 1rkc³⁸), which both adopt the α -helical conformation. The simulations were performed under AMBER99SB-ILDN force field⁴⁸ using TIP3P⁷⁰ water model. The initial VBS molecule was immersed in periodic cuboid water box filled with 0.15 M NaCl solution. A cutoff distance of 1 nm was applied to the Lennard-Jones interactions and short-range electrostatic interactions. Long-range electrostatic interactions were calculated using Particle-Mesh Ewald (PME) method with a grid spacing of 0.16 nm and 4th order interpolation.

500 steps of steepest descent energy minimization were performed to the simulation system to ensure a reasonable starting structure. Thereafter the energetically minimized system was subjected to a 100-ps NVT equilibration heating and stabilizing the system at 300 K; followed by a 100-ps NPT equilibration stabilizing the pressure of the system. Upon completion of energy minimization and two-step equilibration, 1- μ s MD simulation was performed during which the system coordinates were stored every 10 ps for further analysis.

To apply constant force (7 pN and 20 pN) to the VBS molecule in MD simulation, the N-terminal residue was fixed and C-terminal residue was subject to the corresponding constant force.

Dihedral angle principal component analysis (dPCA) and free energy landscape

Principal component analysis (PCA) is a dimensionality-reduction method used to identify and retain the most important degrees of freedom of a dynamic

simulation system^{71, 72}. dPCA has been developed to use the sine and cosine transformed backbone dihedral angles as internal coordinates in the PCA of the MD simulations⁴⁹.

In this work, 60 peptide backbone dihedral angles of the 32-aa R6 VBS peptide, as well as 48 peptide backbone dihedral angles of the 26-aa R10 VBS peptide were used to perform the dPCA. Upon extraction of the dihedral angles from simulation trajectory and implementation of sine and cosine transformation of the dihedral angles, covariance matrix can be calculated based on the sine and cosine variables obtained from the trajectory of dihedral angles. By diagonalizing the covariance matrix, eigenvectors Vec_i and eigenvalues λ_i can be obtained and organized in an eigenvalue-descending order, which means λ_1 represents the largest eigenvalue. Thereafter in this work, the first two eigenvectors Vec_1 and Vec_2 associated with the first two largest eigenvalues (i.e., the first two principal components) were chosen to recast the simulation data by projecting the data onto Vec_1 and Vec_2 .

Subsequently, the free energy landscape along the first two principal components can be expressed by $\Delta G(Vec_1, Vec_2) = -k_B T \ln \frac{P(Vec_1, Vec_2)}{P_{max}}$, where k_B is the Boltzmann constant, T is the temperature, $P(Vec_1, Vec_2)$ refers to the probability distribution of the system around (Vec_1, Vec_2) , and P_{max} is the maximum value of the probability distribution.

Protein secondary structure assignments by DSSP (Dictionary of Protein Secondary Structure)

DSSP is an algorithm assigning secondary structure to the protein residues on the basis of hydrogen bond patterns⁵⁰. The DSSP defines 8 types of secondary structures: α -helix, 3_{10} helix, π -helix, hydrogen bonded turn, β -sheet, β -bridge, bend, and coil. In this work, the secondary structure of VBS residues were analyzed by using GROMACS do_dssp command with calling the dssp program.

Fluorescence polarization assay

A peptide corresponding to helix 27 of talin (residues 1324-1359) was synthesized by GLBiochem (China) TDPASP NLKSQLAAAARAVTDSINQLITM CTQQAPG. The peptide was coupled to a thiol-reactive fluorescein dye via the cysteine and stock solution made in phosphate-buffered saline (PBS; 137 mM NaCl, 27 mM KCl, 100 mM Na₂HPO₄, 18 mM KH₂PO₄, pH 7.4), 1 mM TCEP and 0.05% Triton X-100. Excess dye was removed using a PD-10 desalting column (GE Healthcare, Chicago, IL, USA). The titration was performed in PBS using a constant 1 μ M concentration of peptide with increasing concentration of protein; final volume 100 μ L in a black 96-well plate. Fluorescent polarization (FP) measurements were recorded on a BMGLabTech CLARIOstar plate reader at room temperature and analyzed using GraphPad Prism. The details of fitting function to determine the K_d value can be found in Supp. Info. 4.

Supporting Information

Supplementary Information 1-5;
Supplementary Figures 1-4;
Supplementary Box 1.

Acknowledgements

We thank David Critchley for critical reading of the manuscript. J. Y. was funded by the Singapore Ministry of Education Academic Research Fund Tier 2 (MOE2019-T2-1-099) and the Ministry of Education under the Research Centres of Excellence programme. B.T.G. was funded by BBSRC (BB/N007336/1 and BB/S007245/1). B.T.G. and J.Y. were funded by HFSP (RGP00001/2016).

Author contributions

Y.W. carried out the single-molecule experiments and molecular dynamics simulations. Y.W., M.Y. and S.L. performed data analysis. Y.W., M.Y., K.B.B., R.E.G. and S.L. contributed to the design and expression of the protein constructs for single-molecule experiments. Y.W., J.Y., and B.T.G. interpreted the experimental and simulation data. J.Y. and B.T.G. supervised the research. Y.W., J.Y. and B.T.G. wrote the paper.

Competing Interests statement

The authors declare no competing interest.

References

1. Horwitz, A.; Duggan, K.; Buck, C.; Beckerle, M. C.; Burridge, K., Interaction of plasma membrane fibronectin receptor with talin—a transmembrane linkage. *Nature* **1986**, *320* (6062), 531-533.
2. Burridge, K.; Mangeat, P., An interaction between vinculin and talin. *Nature* **1984**, *308* (5961), 744-746.
3. Johnson, R. P.; Craig, S. W., F-actin binding site masked by the intramolecular association of vinculin head and tail domains. *Nature* **1995**, *373* (6511), 261-264.
4. Humphries, J. D.; Wang, P.; Streuli, C.; Geiger, B.; Humphries, M. J.; Ballestrem, C., Vinculin controls focal adhesion formation by direct interactions with talin and actin. *The Journal of cell biology* **2007**, *179* (5), 1043-1057.
5. Edelman, G. M., Cell adhesion molecules in the regulation of animal form and tissue pattern. *Annual review of cell biology* **1986**, *2* (1), 81-116.
6. Mammoto, T.; Ingber, D. E., Mechanical control of tissue and organ development. *Development* **2010**, *137* (9), 1407-1420.
7. Calderwood, D. A.; Zent, R.; Grant, R.; Rees, D. J. G.; Hynes, R. O.; Ginsberg, M. H., The talin head domain binds to integrin β subunit cytoplasmic tails and regulates integrin activation. *Journal of Biological Chemistry* **1999**, *274* (40), 28071-28074.
8. Goult, B. T.; Bouaouina, M.; Elliott, P. R.; Bate, N.; Patel, B.; Gingras, A. R.; Grossmann, J. G.; Roberts, G. C.; Calderwood, D. A.; Critchley, D. R., Structure of a double ubiquitin - like domain in the talin head: a role in integrin activation. *The EMBO journal* **2010**, *29* (6), 1069-1080.
9. Giannone, G.; Jiang, G.; Sutton, D. H.; Critchley, D. R.; Sheetz, M. P., Talin1 is critical for force-dependent reinforcement of initial integrin–cytoskeleton bonds but not tyrosine kinase activation. *The Journal of cell biology* **2003**, *163* (2), 409-419.
10. Kanchanawong, P.; Shtengel, G.; Pasapera, A. M.; Ramko, E. B.; Davidson, M. W.; Hess, H. F.; Waterman, C. M., Nanoscale architecture of integrin-based cell adhesions. *Nature* **2010**, *468* (7323), 580-584.
11. Margadant, F.; Chew, L. L.; Hu, X.; Yu, H.; Bate, N.; Zhang, X.; Sheetz, M., Mechanotransduction in vivo by repeated talin stretch-relaxation events depends upon vinculin. *PLoS biology* **2011**, *9* (12), e1001223.

- 1
2
3
4
5
6
7
8
9
10
11
12
13
14
15
16
17
18
19
20
21
22
23
24
25
26
27
28
29
30
31
32
33
34
35
36
37
38
39
40
41
42
43
44
45
46
47
48
49
50
51
52
53
54
55
56
57
58
59
60
12. Austen, K.; Ringer, P.; Mehlich, A.; Chrostek-Grashoff, A.; Kluger, C.; Klingner, C.; Sabass, B.; Zent, R.; Rief, M.; Grashoff, C., Extracellular rigidity sensing by talin isoform-specific mechanical linkages. *Nature cell biology* **2015**, *17* (12), 1597-1606.
13. Kumar, A.; Ouyang, M.; Van den Dries, K.; McGhee, E. J.; Tanaka, K.; Anderson, M. D.; Groisman, A.; Goult, B. T.; Anderson, K. I.; Schwartz, M. A., Talin tension sensor reveals novel features of focal adhesion force transmission and mechanosensitivity. *Journal of Cell Biology* **2016**, *213* (3), 371-383.
14. Del Rio, A.; Perez-Jimenez, R.; Liu, R.; Roca-Cusachs, P.; Fernandez, J. M.; Sheetz, M. P., Stretching single talin rod molecules activates vinculin binding. *Science* **2009**, *323* (5914), 638-641.
15. Yao, M.; Goult, B. T.; Chen, H.; Cong, P.; Sheetz, M. P.; Yan, J., Mechanical activation of vinculin binding to talin locks talin in an unfolded conformation. *Scientific reports* **2014**, *4* (1), 1-7.
16. Yao, M.; Goult, B. T.; Klapholz, B.; Hu, X.; Toseland, C. P.; Guo, Y.; Cong, P.; Sheetz, M. P.; Yan, J., The mechanical response of talin. *Nature communications* **2016**, *7* (1), 1-11.
17. Hu, X.; Jing, C.; Xu, X.; Nakazawa, N.; Cornish, V. W.; Margadant, F. M.; Sheetz, M. P., Cooperative vinculin binding to talin mapped by time-resolved super resolution microscopy. *Nano letters* **2016**, *16* (7), 4062-4068.
18. Goult, B. T.; Yan, J.; Schwartz, M. A., Talin as a mechanosensitive signaling hub. *Journal of Cell Biology* **2018**, *217* (11), 3776-3784.
19. Ciobanasu, C.; Faivre, B.; Le Clainche, C., Actomyosin-dependent formation of the mechanosensitive talin-vinculin complex reinforces actin anchoring. *Nature communications* **2014**, *5* (1), 1-10.
20. Vigouroux, C.; Henriot, V.; Le Clainche, C., Talin dissociates from RIAM and associates to vinculin sequentially in response to the actomyosin force. *Nature communications* **2020**, *11* (1), 1-11.
21. Wen, K.-K.; Rubenstein, P. A.; DeMali, K. A., Vinculin nucleates actin polymerization and modifies actin filament structure. *Journal of Biological Chemistry* **2009**, *284* (44), 30463-30473.
22. Bays, J. L.; DeMali, K. A., Vinculin in cell-cell and cell-matrix adhesions. *Cellular and Molecular Life Sciences* **2017**, *74* (16), 2999-3009.
23. Bakolitsa, C.; Cohen, D. M.; Bankston, L. A.; Bobkov, A. A.; Cadwell, G. W.; Jennings, L.; Critchley, D. R.; Craig, S. W.; Liddington, R. C., Structural basis for vinculin activation at sites of cell adhesion. *Nature* **2004**, *430* (6999), 583-586.
24. Borgon, R. A.; Vornrhein, C.; Bricogne, G.; Bois, P. R.; Izard, T., Crystal structure of human vinculin. *Structure* **2004**, *12* (7), 1189-1197.
25. Brindle, N. P.; Holt, M. R.; Davies, J. E.; Price, C. J.; Critchley, D. R., The focal-adhesion vasodilator-stimulated phosphoprotein (VASP) binds to the proline-rich domain in vinculin. *Biochemical Journal* **1996**, *318* (3), 753-757.
26. DeMali, K. A.; Barlow, C. A.; Burridge, K., Recruitment of the Arp2/3 complex to vinculin: coupling membrane protrusion to matrix adhesion. *The Journal of cell biology* **2002**, *159* (5), 881-891.
27. Atherton, P.; Lausecker, F.; Carisey, A.; Gilmore, A.; Critchley, D.; Barsukov, I.; Ballestrem, C., Relief of talin autoinhibition triggers a force-independent association with vinculin. Mechanisms of talin and vinculin interactions. *The Journal of Cell Biology* **2020**, *219* (1), e201903134.
28. Kelley, C. F.; Litschel, T.; Schumacher, S.; Dedden, D.; Schwille, P.; Mizuno, N., Phosphoinositides regulate force-independent interactions between

- 1
2
3 talin, vinculin, and actin. *Elife* **2020**, *9*,
4 e56110.
5
6 29. Boujemaa-Paterski, R.; Martins, B.;
7 Eibauer, M.; Beales, C. T.; Geiger, B.;
8 Medalia, O., Talin-activated vinculin
9 interacts with branched actin networks to
10 initiate bundles. *Elife* **2020**, *9*, e53990.
11
12 30. Han, S. J.; Azarova, E. V.;
13 Whitewood, A. J.; Bachir, A.; Guttierrez, E.;
14 Groisman, A.; Horwitz, A. R.; Goult, B. T.;
15 Dean, K. M.; Danuser, G., Pre-
16 complexation of talin and vinculin without
17 tension is required for efficient nascent
18 adhesion maturation. *Elife* **2021**, *10*,
19 e66151.
20
21 31. Goult, B. T.; Zacharchenko, T.; Bate,
22 N.; Tsang, R.; Hey, F.; Gingras, A. R.; Elliott,
23 P. R.; Roberts, G. C.; Ballestrem, C.;
24 Critchley, D. R., RIAM and vinculin binding
25 to talin are mutually exclusive and regulate
26 adhesion assembly and turnover. *Journal*
27 *of Biological Chemistry* **2013**, *288* (12),
28 8238-8249.
29
30 32. Bois, P. R.; O'Hara, B. P.;
31 Nietlispach, D.; Kirkpatrick, J.; Izard, T., The
32 vinculin binding sites of talin and α -actinin
33 are sufficient to activate vinculin. *Journal*
34 *of Biological Chemistry* **2006**, *281* (11),
35 7228-7236.
36
37 33. Wang, Y.; Yan, J.; Goult, B. T.,
38 Force-dependent binding constants. *Biochemistry* **2019**, *58* (47), 4696-4709.
39
40 34. Dahlke, K.; Zhao, J.; Sing, C. E.;
41 Banigan, E. J., Force-dependent facilitated
42 dissociation can generate protein-DNA
43 catch bonds. *Biophysical journal* **2019**, *117*
44 (6), 1085-1100.
45
46 35. Cohen, D. M.; Chen, H.; Johnson, R.
47 P.; Choudhury, B.; Craig, S. W., Two
48 distinct head-tail interfaces cooperate to
49 suppress activation of vinculin by talin.
50 *Journal of Biological Chemistry* **2005**, *280*
51 (17), 17109-17117.
52
53 36. Johnson, R. P.; Craig, S. W., An
54 intramolecular association between the
55 head and tail domains of vinculin
56 modulates talin binding. *Journal of*
57 *Biological Chemistry* **1994**, *269* (17),
58 12611-12619.
59
60 37. Chen, H.; Choudhury, D. M.; Craig,
S. W., Coincidence of actin filaments and
talin is required to activate vinculin.
Journal of Biological Chemistry **2006**, *281*
(52), 40389-40398.
38. Izard, T.; Evans, G.; Borgon, R. A.;
Rush, C. L.; Bricogne, G.; Bois, P. R.,
Vinculin activation by talin through helical
bundle conversion. *Nature* **2004**, *427*
(6970), 171-175.
39. Izard, T.; Vornrhein, C., Structural
basis for amplifying vinculin activation by
talin. *Journal of Biological Chemistry* **2004**,
279 (26), 27667-27678.
40. Pasapera, A. M.; Schneider, I. C.;
Rericha, E.; Schlaepfer, D. D.; Waterman,
C. M., Myosin II activity regulates vinculin
recruitment to focal adhesions through
FAK-mediated paxillin phosphorylation.
Journal of Cell Biology **2010**, *188* (6), 877-
890.
41. Stutchbury, B.; Atherton, P.; Tsang,
R.; Wang, D.-Y.; Ballestrem, C., Distinct
focal adhesion protein modules control
different aspects of mechanotransduction.
Journal of cell science **2017**, *130* (9), 1612-
1624.
42. Lemke, S. B.; Weidemann, T.; Cost,
A.-L.; Grashoff, C.; Schnorrer, F., A small
proportion of Talin molecules transmit
forces at developing muscle attachments
in vivo. *PLoS biology* **2019**, *17* (3),
e3000057.
43. Yao, M.; Qiu, W.; Liu, R.; Efremov,
A. K.; Cong, P.; Seddiki, R.; Payre, M.; Lim,
C. T.; Ladoux, B.; Mege, R.-M., Force-
dependent conformational switch of α -
catenin controls vinculin binding. *Nature*
communications **2014**, *5* (1), 1-12.
44. Pang, S. M.; Le, S.; Kwiatkowski, A.
V.; Yan, J., Mechanical stability of α T-
catenin and its activation by force for
vinculin binding. *Molecular biology of the*
cell **2019**, *30* (16), 1930-1937.

- 1
2
3
4
5
6
7
8
9
10
11
12
13
14
15
16
17
18
19
20
21
22
23
24
25
26
27
28
29
30
31
32
33
34
35
36
37
38
39
40
41
42
43
44
45
46
47
48
49
50
51
52
53
54
55
56
57
58
59
60
45. Zhao, X.; Zeng, X.; Lu, C.; Yan, J., Studying the mechanical responses of proteins using magnetic tweezers. *Nanotechnology* **2017**, *28* (41), 414002.
46. Berg, O. G.; von Hippel, P. H., Diffusion-controlled macromolecular interactions. *Annual review of biophysics and biophysical chemistry* **1985**, *14* (1), 131-158.
47. Chorev, D. S.; Volberg, T.; Livne, A.; Eisenstein, M.; Martins, B.; Kam, Z.; Jockusch, B. M.; Medalia, O.; Sharon, M.; Geiger, B., Conformational states during vinculin unlocking differentially regulate focal adhesion properties. *Scientific reports* **2018**, *8* (1), 1-14.
48. Lindorff - Larsen, K.; Piana, S.; Palmo, K.; Maragakis, P.; Klepeis, J. L.; Dror, R. O.; Shaw, D. E., Improved side-chain torsion potentials for the Amber ff99SB protein force field. *Proteins: Structure, Function, and Bioinformatics* **2010**, *78* (8), 1950-1958.
49. Mu, Y.; Nguyen, P. H.; Stock, G., Energy landscape of a small peptide revealed by dihedral angle principal component analysis. *Proteins: Structure, Function, and Bioinformatics* **2005**, *58* (1), 45-52.
50. Kabsch, W.; Sander, C., Dictionary of protein secondary structure: pattern recognition of hydrogen - bonded and geometrical features. *Biopolymers: Original Research on Biomolecules* **1983**, *22* (12), 2577-2637.
51. Khan, R. B.; Goult, B. T., Adhesions Assemble!—Autoinhibition as a Major Regulatory Mechanism of Integrin-Mediated Adhesion. *Frontiers in molecular biosciences* **2019**, *6*, 144.
52. Goult, B. T.; Xu, X.-P.; Gingras, A. R.; Swift, M.; Patel, B.; Bate, N.; Kopp, P. M.; Barsukov, I. L.; Critchley, D. R.; Volkman, N., Structural studies on full-length talin1 reveal a compact auto-inhibited dimer: implications for talin activation. *Journal of structural biology* **2013**, *184* (1), 21-32.
53. Dedden, D.; Schumacher, S.; Kelley, C. F.; Zacharias, M.; Biertümpfel, C.; Fässler, R.; Mizuno, N., The architecture of Talin1 reveals an autoinhibition mechanism. *Cell* **2019**, *179* (1), 120-131. e13.
54. Han, S.; Dean, K.; Whitewood, J.; Bachir, A.; Guttierrez, E.; Groisman, A.; Horwitz, A.; Goult, B.; Danuser, G., Formation of talin-vinculin pre-complexes dictates maturation of nascent adhesions by accelerated force transmission and vinculin recruitment. bioRxiv: 735183. 2019.
55. Carisey, A.; Tsang, R.; Greiner, A. M.; Nijenhuis, N.; Heath, N.; Nazgiewicz, A.; Kemkemer, R.; Derby, B.; Spatz, J.; Ballestrem, C., Vinculin regulates the recruitment and release of core focal adhesion proteins in a force-dependent manner. *Current biology* **2013**, *23* (4), 271-281.
56. Maartens, A. P.; Wellmann, J.; Wictome, E.; Klapholz, B.; Green, H.; Brown, N. H., Drosophila vinculin is more harmful when hyperactive than absent, and can circumvent integrin to form adhesion complexes. *J Cell Sci* **2016**, *129* (23), 4354-4365.
57. Auernheimer, V.; Lautscham, L. A.; Leidenberger, M.; Friedrich, O.; Kappes, B.; Fabry, B.; Goldmann, W. H., Vinculin phosphorylation at residues Y100 and Y1065 is required for cellular force transmission. *Journal of cell science* **2015**, *128* (18), 3435-3443.
58. Zhang, Z.; Izaguirre, G.; Lin, S.-Y.; Lee, H. Y.; Schaefer, E.; Haimovich, B., The phosphorylation of vinculin on tyrosine residues 100 and 1065, mediated by SRC kinases, affects cell spreading. *Molecular biology of the cell* **2004**, *15* (9), 4234-4247.
59. Pelham, R. J.; Wang, Y.-I., Cell locomotion and focal adhesions are regulated by substrate flexibility.

- 1
2
3
4
5
6
7
8
9
10
11
12
13
14
15
16
17
18
19
20
21
22
23
24
25
26
27
28
29
30
31
32
33
34
35
36
37
38
39
40
41
42
43
44
45
46
47
48
49
50
51
52
53
54
55
56
57
58
59
60
- Proceedings of the National Academy of Sciences* **1997**, *94* (25), 13661-13665.
60. Riveline, D.; Zamir, E.; Balaban, N. Q.; Schwarz, U. S.; Ishizaki, T.; Narumiya, S.; Kam, Z.; Geiger, B.; Bershadsky, A. D., Focal contacts as mechanosensors: externally applied local mechanical force induces growth of focal contacts by an mDia1-dependent and ROCK-independent mechanism. *The Journal of cell biology* **2001**, *153* (6), 1175-1186.
61. Gough, R. E.; Goult, B. T., The tale of two talins—two isoforms to fine-tune integrin signalling. *FEBS letters* **2018**, *592* (12), 2108-2125.
62. Changede, R.; Xu, X.; Margadant, F.; Sheetz, M. P., Nascent integrin adhesions form on all matrix rigidities after integrin activation. *Developmental cell* **2015**, *35* (5), 614-621.
63. Gough, R. E.; Jones, M. C.; Zacharchenko, T.; Le, S.; Yu, M.; Jacquemet, G.; Muench, S. P.; Yan, J.; Humphries, J. D.; Jørgensen, C.; Humphries, M. J.; Goult, B. T., Talin mechanosensitivity is modulated by a direct interaction with cyclin-dependent kinase-1. *bioRxiv* **2021**, 2021.03.19.436208.
64. Goult, B. T., The Mechanical Basis of Memory—the MeshCODE Theory. *Frontiers in Molecular Neuroscience* **2021**, *14*, 21.
65. Khan, R. B.; Varela, L.; Cowell, A. R.; Goult, B. T., Biochemical Characterization of the Integrin Interactome. In *The Integrin Interactome*, Springer: 2020; pp 115-147.
66. Chen, H.; Fu, H.; Zhu, X.; Cong, P.; Nakamura, F.; Yan, J., Improved high-force magnetic tweezers for stretching and refolding of proteins and short DNA. *Biophysical journal* **2011**, *100* (2), 517-523.
67. Efron, B.; Tibshirani, R. J., *An introduction to the bootstrap*. CRC press: **1994**, 45-57.
68. Berendsen, H. J.; van der Spoel, D.; van Drunen, R., GROMACS: a message-passing parallel molecular dynamics implementation. *Computer physics communications* **1995**, *91* (1-3), 43-56.
69. Abraham, M. J.; Murtola, T.; Schulz, R.; Páll, S.; Smith, J. C.; Hess, B.; Lindahl, E., GROMACS: High performance molecular simulations through multi-level parallelism from laptops to supercomputers. *SoftwareX* **2015**, *1*, 19-25.
70. Jorgensen, W. L.; Chandrasekhar, J.; Madura, J. D.; Impey, R. W.; Klein, M. L., Comparison of simple potential functions for simulating liquid water. *The Journal of chemical physics* **1983**, *79* (2), 926-935.
71. Ichiye, T.; Karplus, M., Collective motions in proteins: a covariance analysis of atomic fluctuations in molecular dynamics and normal mode simulations. *Proteins: Structure, Function, and Bioinformatics* **1991**, *11* (3), 205-217.
72. García, A. E., Large-amplitude nonlinear motions in proteins. *Physical review letters* **1992**, *68* (17), 2696.

TOC Graphic

